Liu Hanlong, Deng An, Shen Yang
Shear behavior of coarse aggregates for dam construction under varied stress paths
Water Science and Engineering, 2008; 1(1):63-77

http://dx.doi.org/10.3882/j.issn.1674-2370.2008.01.007

Shear Behavior of Coarse Dam Aggregates under High Confining Pressures and Varied Stress Paths

(1. Key Laboratory of Ministry of Education for Geomechanics and Embankment Engineering, Hohai University, Nanjing 210098；
2.Geotechnical Research Institute, Hohai University, Nanjing 210098)

The work is supported by a grant (No. 50639050) from National Natural Science Foundation of China.

Abstract

Coarse aggregates are the major infrastructure materials of concrete slab rock-fill dams and are consolidated to bear upper and lateral loads. With the increase of dam height, high confining pressures and complex stress states complicate the shear behavior of coarse aggregates, and thus impede the high dam's proper construction, operations and maintenance. An experimental program was launched to study the shear behavior of coarse dam aggregates using a large-scale triaxial shear apparatus. Using conventional triaxial shear tests, aggregate's strain-stress behaviors under high constant confining pressures, i.e. 300, 600, 900 and 1200 kPa, were observed. Shear strengths and aggregate breakage characteristics associated with the high pressure shear processes were discussed. Stress path tests, i.e. constant p tests, constant q tests and constant η tests, were conducted to observe and analyze coarse aggregate response under complex stress states. It was found that peak deviator stress $(\sigma_1' - \sigma_3')_p$ increases with confining pressure σ_3' increase, whereas peak principal stress ratio $(\sigma_1'/\sigma_3')_p$ decrease with confining pressure σ_3' increase. With confining pressure increase, the dilation decreases and the contraction eventually prevails. Initial strength parameters (Poisson's ratio υ_i and tangent modulus E_i) presents a nonlinear relationship with confining pressures, if the pressure is relatively low. Shear strength parameters decrease with increase confining pressures. The failure

envelope line is a down-deflexed curve, with clear curvature under low confining pressures. Under moderate confining pressures, dilation is offset by particle breakage. Under high confining pressures, dilation disappears.

Keywords: coarse aggregate, large-scale triaxial shear test, high confining pressure, stress path, stress-strain behavior, breakage.

Introduction

Concrete-slab rock-fill dams are being built at increasing heights. In mid-west China, 134 rock-fill dams of over 200 m is planned to be built in the next two decades. The height of rock-fill dams has increased from on average 100 m to over 200 m. The three-gorge dam, 375 m in height, was already put into use. With the increase of dam height, both the confining pressures and the stress states are different from those of low dams. As the base materials of low dams, coarse aggregates are generally subjected to a confining pressure less than 400 kPa. For a 200 m high dam, however, the confining pressure climbs over 800 kPa. In addition, due to the complex construction procedures and varied reservoir water table associated with high dams, the stress states, e.g. loading-unloading-reloading, on aggregates are more complicated compared to those under low height dams. Thus, coarse aggregates for high dams may demonstrate different shear behavior, which renders the issue of building a new constitutive model for high dam coarse aggregates. Before a valid constitutive

model is proposed, it becomes paramount to research shear behaviors of coarse aggregates under high confining pressures and complex stress states.

Many studies were conducted on coarse aggregate shear behaviors under low confining pressures, e.g., low rock-fill dams and railway bases (Wang 1999). All these studies nicely described aggregate shear strengths. Less experimental works, however, were performed with regards to coarse aggregate shear behavior under high confining pressures and complex stress states.

An experimental study, using a large-scale triaxial shear apparatus, was conducted on coarse aggregates to obtain concise observation and analyses documenting coarse aggregate shear behaviors. Conventional triaxial shear tests and stress path tests were performed. The tests focused on the shear strengths and deformation behavior of coarse aggregates under varied confining pressures, i.e, 300, 600, 900 and 1200 kPa, the effect of varied stress paths on shear strength and deformation, the aggregate breakage characteristics and its effect on aggregate shear behavior, the effect of mudstone contents on shear behavior. Observations from stress path tests provide technical parameters suitable for various construction states and help assess the behavior of coarse aggregates under complex stress paths.

Experimental Program

Materials

Coarse aggregates were retrieved from a pumped storage power station located at Yi-xing east China. The aggregate is identified as moderate weathered quartz sandstones containing 10-15% mudstones. The maximum grain size of in-situ coarse aggregate is 800 mm and exceeds the specimen dimension limits designed for a large-scale shear apparatus. A scaling on aggregate gradation was implemented. Currently, three methods are available for treating out-of-limit aggregates in shear tests, i.e. scalping method, gradation-simulating method and mass balanced method (Indraratna et al. 1998). The scalping method leads to an increased portion of fine grains and thus affects the properties of coarse aggregates. A better alternative method is to combine gradation-simulating method and mass balanced method to scale a specimen (Indraratna et al. 1998). In this study, the combined method was used. First, the aggregate gradation was scaled to a half of the initial sizes. Then a mass balanced method was used and the percentage of grains less than 5 mm was kept constant. The initial designed gradation of coarse aggregates and scaled gradation for specimens are presented in Fig. 1. The sizes of scaled aggregates range from 60 to 1 mm, which enables the fitting of aggregates into the shear apparatus.

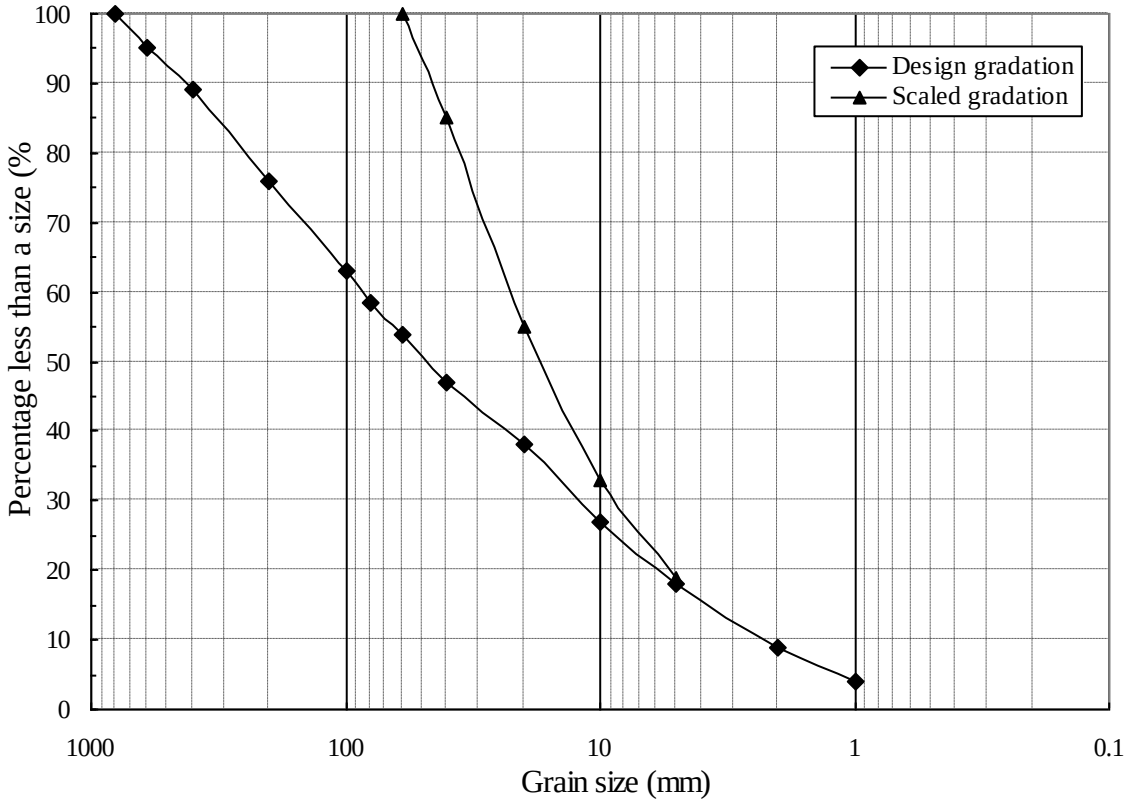

Fig. 1: Gradation curves of designed coarse aggregates and scaled specimens.

Large-scale triaxial shear apparatus

Model YS-30 stress path large-scale triaxial shear apparatus is used in this study. Fig. 2 demonstrates its pressure cell. Pressure is oil-controlled. An auto-switch panel controls the oil flows as well as confining pressures. The confining pressure is able to reach up to 3.0 MPa and is observed in terms of the pressure gauges attached to the oil-pressure system. Measurements of the axial stresses and strains are obtained by using instrumented pressure sensors and displacement sensors. Pore water pressure is measured by using a membranous sensitive pore

water sensor (piezometer) attached to the cell base. Data acquisitions cover following parameters: axial stresses and strains, confining pressures, pore water pressures, volumetric strain, reverse pressures and volumetric strain. All measurements are basically automatic by running the control panel.

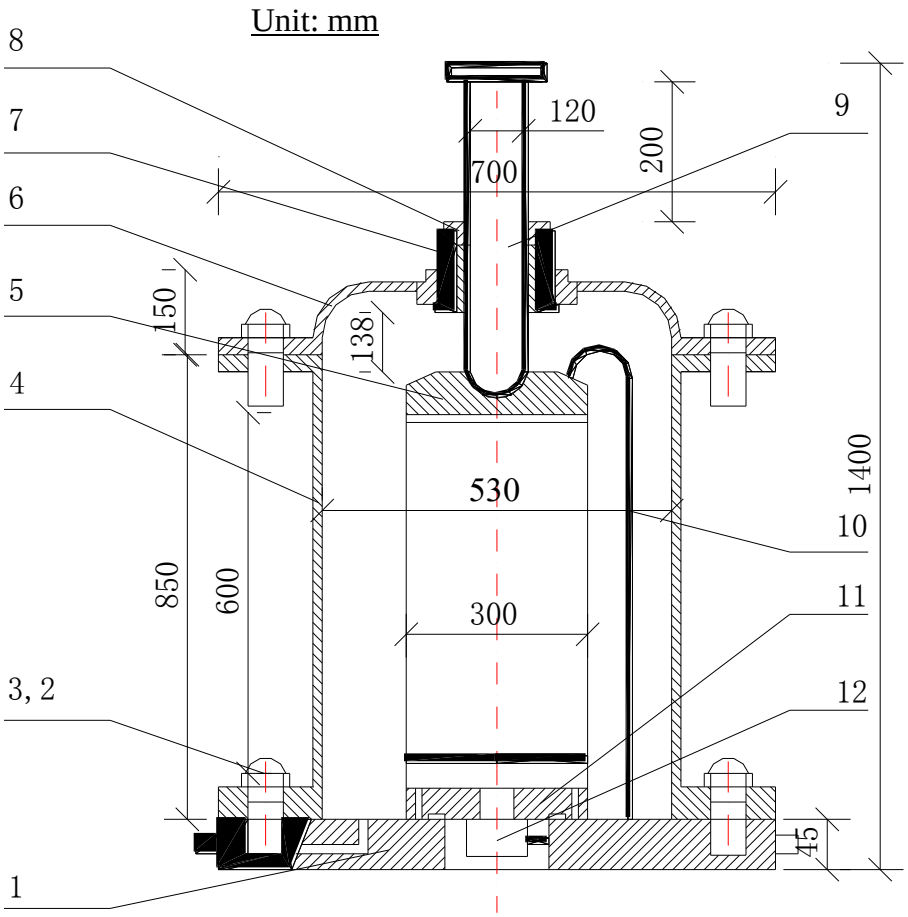

1—base, 2—screw, 3—pad, 4—cylinder external wall, 5—specimen cap, 6—cylinder cap, 7—shaft-piston combination, 8—auxiliary cap, 9—shaft, 10—cap connector, 11—load sensor, 12—pressure moderator.

Fig. 2: Schematic of large-scale shear apparatus shear chamber.

Specimen preparation

The coarse aggregates were placed in layers into the cylinder. Three layers of scaled aggregates were placed and compacted to designed dry density (2.12 g/cm^3). The cylinder is splittable and forms a specimen dimension of Ø300×600 mm. Around 100 kg coarse aggregates were needed to fill the cylinder in a batch test. In consideration of the angular shapes of coarse aggregates, thin rubber pads were sandwiched between the water-proof membrane and specimens to avoid membrane punctuation. Slight confining effects were provided by the rubber pads. After filling coarse aggregates, a combination of vacuum pumping and water head saturation was used to saturate specimens. The water was sucked upwards till it overflows the cylindrical specimens for 20 minutes. A small confining pressure of less than 20 kPa was applied when the water head saturation method was conducted. A pore water pressure coefficient of 0.95 or higher indicates specimen saturation.

In this study, two mass percentages of mudstone ratios are considered, i.e. 10% and 15%, to observe the effect of mudstone percentage on shear behavior of coarse aggregates. Two groups of specimens are prepared addressing 10% and 15% mudstone contents, respectively. MS10 and MS15 represent each group specimens.

Testing procedures

Conventional consolidated-drained (CD) triaxial shear tests were performed. Four specimens were prepared in a shear test group, corresponding to confining pressures σ_3 of 300, 600, 900 and 1200 kPa, respectively. After the specimen saturation, a confining pressure was applied to consolidate the specimen. When a constant drainage occurs and pore water pressures are consistent with the initial pore water pressures, the specimens are preliminarily consolidated and ready for axial loading. The axial loading is strain-controlled at a rate of 2 mm/min. The excess pore water pressures were maintained close to zero during the shear processes. The shear parameters, i.e. principle strains, principle stresses, deviator stresses and volumetric strain, were automatically measured and recorded regarding their developments by the shear system. A peak value of axial stress indicates the failure state of a specimen. Otherwise, a 15% axial strain determines the final axial loading and its corresponding axial stress represents the peak axial stress. After the fulfillment of a shear test, the specimen was air-dried and its breakage characteristic was observed and analyzed.

The stress path tests were performed to observe material strength and deformation behaviors under simulated loading conditions. The loading is stress-controlled and applied at the rate of 10 kPa/min. Loading or unloading processes need to appropriately be retarded when stress paths change or unloading starts. The system control panel is able to implement and monitor all lateral and axial loading

or unloading processes in a preset way. Following variables are employed: deviator stress $q = \sigma_1 - \sigma_3$, average total stress $p = (\sigma_1 + 2\sigma_3)/3$, stress ratio $\eta = q/p$, stress gradient $\bar{\eta} = dq/dp$, principal stress ratio $R = \sigma_1/\sigma_3$, principal stress gradient $k = d\sigma_3/d\sigma_1$, deviator shear strain $\varepsilon_s = \varepsilon_a - \varepsilon_v/3$, volumetric strain $\varepsilon_v = \varepsilon_a + 2\varepsilon_3$.

Fig. 3 demonstrates total stress paths in *q*-*p* diagrams for triaxial shear tests. All stress paths were accomplished under drained shear conditions. The k_f line represents the failure criterion. Fig. 3 (a) represents four stress paths after the specimens were subjected to a 900 kPa isotropic consolidation, i.e., constant principal stress gradient k (0.125 and 0.333, respectively), constant *p*, and conventional triaxial compression (maintain σ_3 and increase σ_1). An unloading was followed on *k*=0.333 stress path. These paths help observe the shear behavior of coarse aggregate subjected to varied stress states given an initially isotropic state. Fig. 3 (b) represents isotropically consolidated constant average total stress p stress paths. The consolidation pressure σ_3 was 600, 900 and 1200 kPa, respectively. Unloading was followed on 900 kPa constant p stress path before the specimen fails. Fig. 3 (c) represents anisotropically consolidated loading-unloading stress paths. The specimens were firstly consolidated till consolidation pressure σ_3 being 800 kPa via stress paths of principal stress ratio *R* being 2.5, 3.0 and 3.5, respectively. Then, the axial stress σ_1 was maintained

constant; the radial stress σ_3 was increased and decreased in sequences. It was meant to simulate the rise and fall of reservoir water table. Fig. 3 (d) represents isotropic consolidation stress paths. The consolidation pressures σ_3 were 300, 900 and 1500 kPa, respectively.

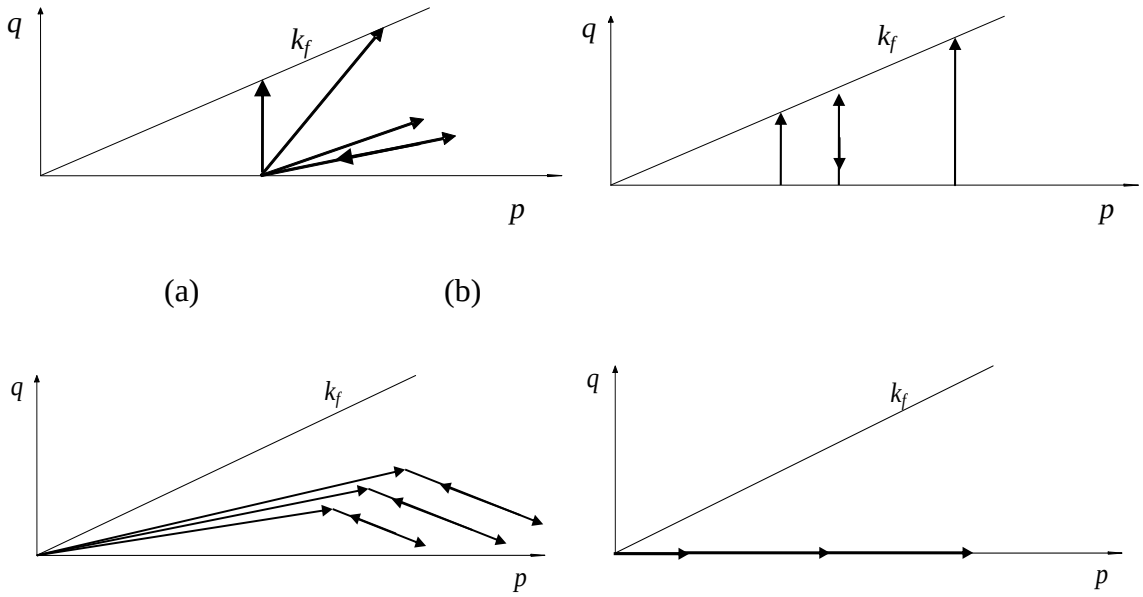

Fig. 3: Total stress paths in *q*-*p* diagrams for triaxial shear tests: (a) isotropically consolidated constant principal stress ratio *R* stress paths, (b) isotropically consolidated constant *p* stress paths, (c) anisotropically consolidated loading-unloading-reloading stress paths, (d) isotropic consolidation stress paths.

Results and Discussion

Stress-strain behaviors

The stress-strain behaviors of coarse aggregates under CD triaxial shear condition are presented in Figs. 4 and 5, corresponding specimens of two mudstone contents, MS10 and MS15, respectively. The depicted behaviors include the curves of deviator stresses $(\sigma_1' - \sigma_3')$ *vs* axial strain ε_a, volumetric strain ε_v *vs* axial strain ε_a, and principal stress ratio (σ_1'/σ_3') *vs* axial strain ε_a. Stress-strain curves for aggregates of two mudstone percentages are similar, which means that coarse aggregate mudstone contents of 10% to 15% do not significantly affect shear stress-strain behaviors of coarse aggregate.

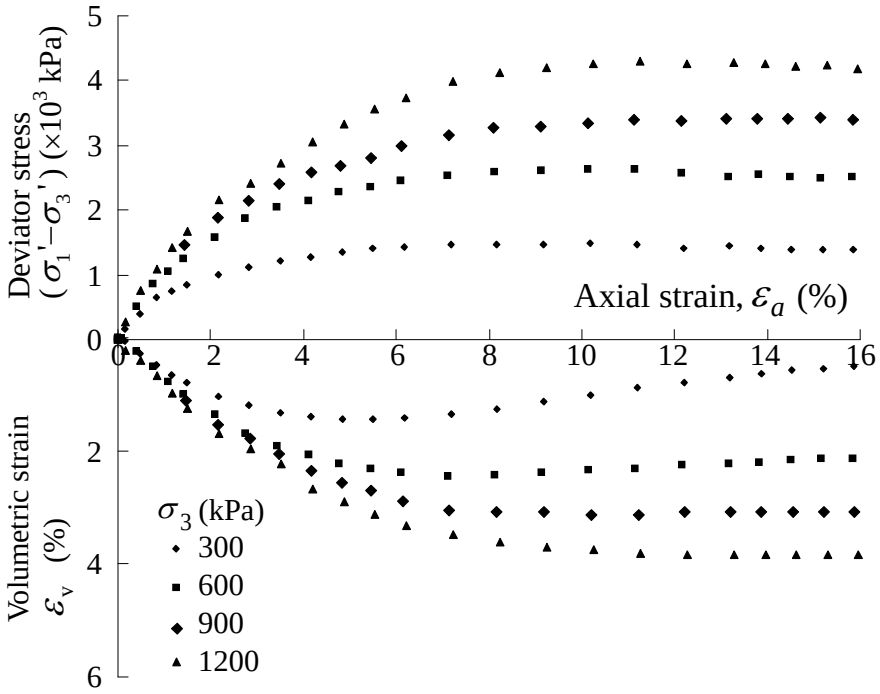

(a)

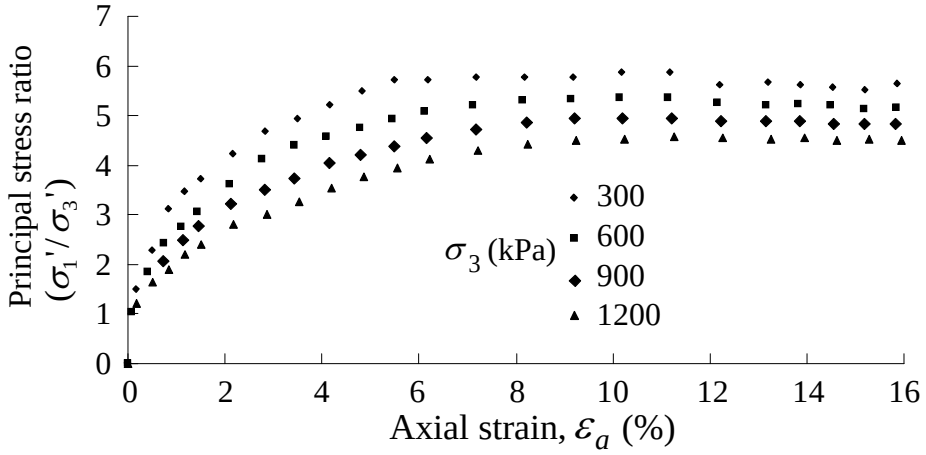

(b)

Fig. 4: Stress-strain behavior during triaxial consolidated-drained shear tests at different confining pressure values on coarse dam aggregate (MS10): (a) variation of deviator stress and volumetric strain with axial strain; (b) influence of confining pressure on ratio of principal effective stresses

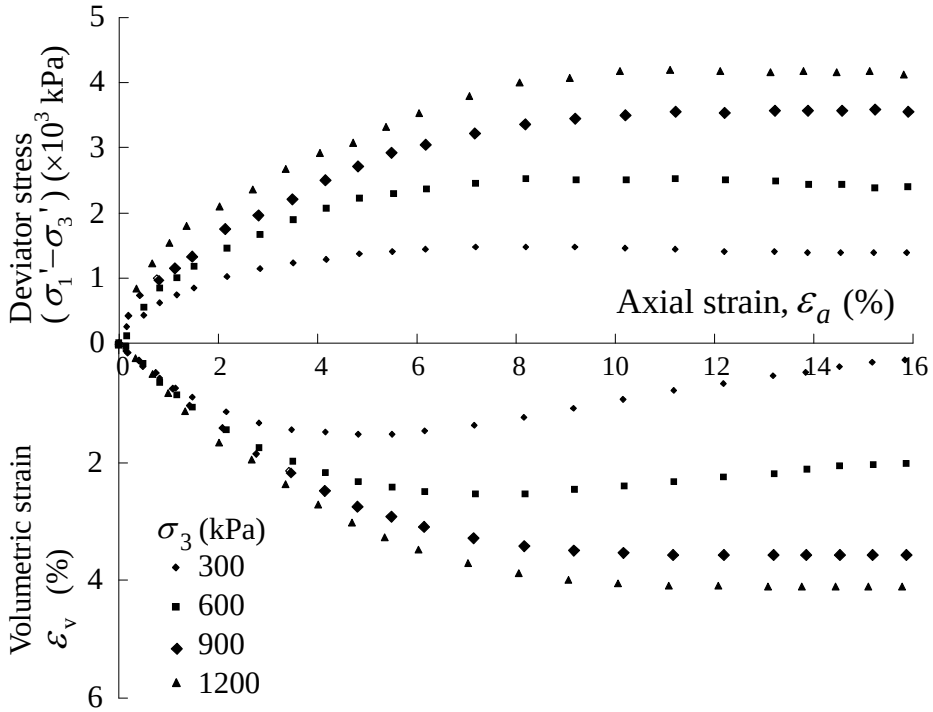

(a)

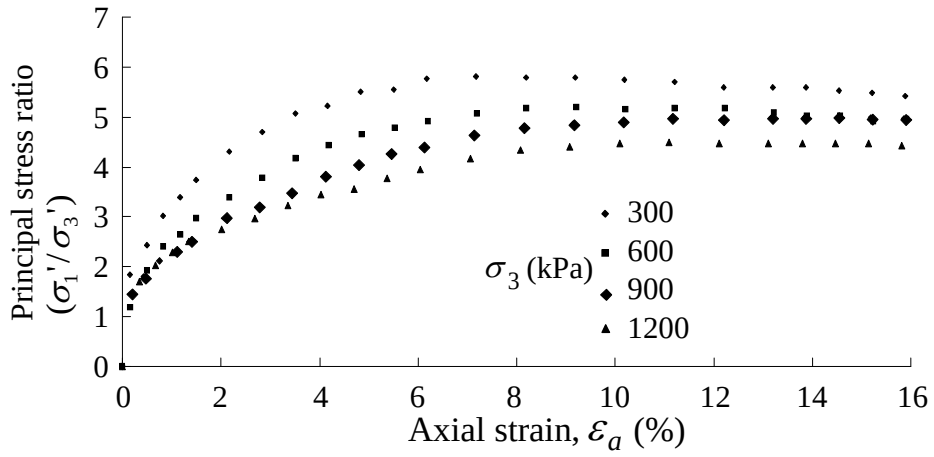

(b)

Fig. 5: Stress-strain behavior during triaxial consolidated-drained shear tests at different confining pressure values on coarse dam aggregate (MS15): (a) variation of deviator stress and volumetric strain with axial strain; (b) influence of confining pressure on ratio of principal effective stresses

It is shown that the peak deviator stress value $(\sigma_1' - \sigma_3')_p$ increases as the confining pressure σ_3' increases, whereas the peak principal stress ratio $(\sigma_1'/\sigma_3')_p$ decreases with the increased confining pressure σ_3'. The findings are in agreement with those for sheared sands and gravels (Bishop 1966)(Vesic and Clough 1968), (Ponce and Bell 1971), dam coarse aggregates (Marsal 1967)(Marsal 1973)(Marachi et al. 1972)(Charles and Watts 1980) and (Indraratna et al. 1993), coarse ballast aggregates under low confining pressures of 1-240 kPa reported by (Indraratna et al. 1998). Indraratna et al. 1998 also reported a peak deviator stress value of 100 to 1200 kPa and a principal stress ratio of 5 to 80 for tested coarse ballast aggregate under low confining pressures. As the confining pressures increase to the levels of 300-1200 kPa (Fig. 4), the

peak deviator stress value drastically increases to a range of 1200 to 4000 kPa, and the peak principal stress ratio drastically decreases to a range of 4 to 6. Combining two investigations, it is inferred that increasing confining pressures σ_3' leads to a increased peak deviator stress value $(\sigma_1' - \sigma_3')_p$ and decreased peak principal stress ratio $(\sigma_1'/\sigma_3')_p$.

Similar stress-strain behavior in triaxial tests is also found associated with other granular materials, e.g., sand, gravel, and dam coarse aggregates (Bishop 1966) (Vesic and Clough 1968) (Ponce and Bell 1971) (Marsal 1967) (Marsal 1973) (Marachi et al. 1972) (Charles and Watts 1980) (Indraratna et al. 1993) (Indraratna et al. 1998). (Indraratna et al. 1998) thought that angular and interlock property of ballast materials under low confining pressures lead to a high $(\sigma_1'/\sigma_3')_p$ value. He also proposed a nonlinear formulation quantifying the relationship between $(\sigma_1'/\sigma_3')_p$ and σ_3'. (Marsal 1973) suggested that the decrease of $(\sigma_1'/\sigma_3')_p$ with increasing σ_3' is related to the aggregate breakage.

Shear contraction $(\varepsilon_v > 0)$ is continually ongoing till the shear processes approach the aggregate failure states when aggregates show limited shear dilation. As the confining pressures increase from 300 to 1200 kPa, the shear dilation becomes weak. For coarse aggregate under relatively low confining pressures at levels of less than 240 kPa (Indraratna et al. 1998), a shear contraction was firstly initiated then significant shear dilation occurred. As the confining pressures

increase from 1 to 240 kPa, the shear dilation tends to be weaker. Coupling the volumetric strain characteristics of coarse aggregate under confining pressures from 1 to 1200 kPa, it is inferred that coarse aggregates undergo shear contraction and shear dilation in sequences. The volumetric strain characteristics are associated with magnitudes of applied confining pressures. Lower confining pressures result in less shear contraction and more shear dilation. Increasing confining pressures tend to intensify shear contraction and mitigate shear dilation. To quantify the volumetric strains per confining pressures, up to 10% volumetric strain of shear dilation occurs under 1 kPa confining pressure according to (Indraratna et al. 1998). Almost none shear dilation were observed when the confining pressure attains 1200 kPa as shown in Figs. 4(a) and 5(a).

Fig. 6 demonstrates the peak values of axial strain, lateral strain and volumetric strain with confining pressure values σ_3' when the specimens attain their fail states. Volumetric contraction strain is observed linear with confining pressures. (Indraratna et al. 1998) reported a transition point at σ_3' of 60 kPa where coarse aggregates become shear contraction from shear dilation. Peak radial strain ε_{rp} is around 3.5% for the applied confining pressure ranges (300-1200 kPa), lower than ε_{rp} of around 5% for less confining pressures (1-240 kPa) reported by (Indraratna et al. 1998). No rupture plane was identified, but a symmetrical bulging was observed at failure.

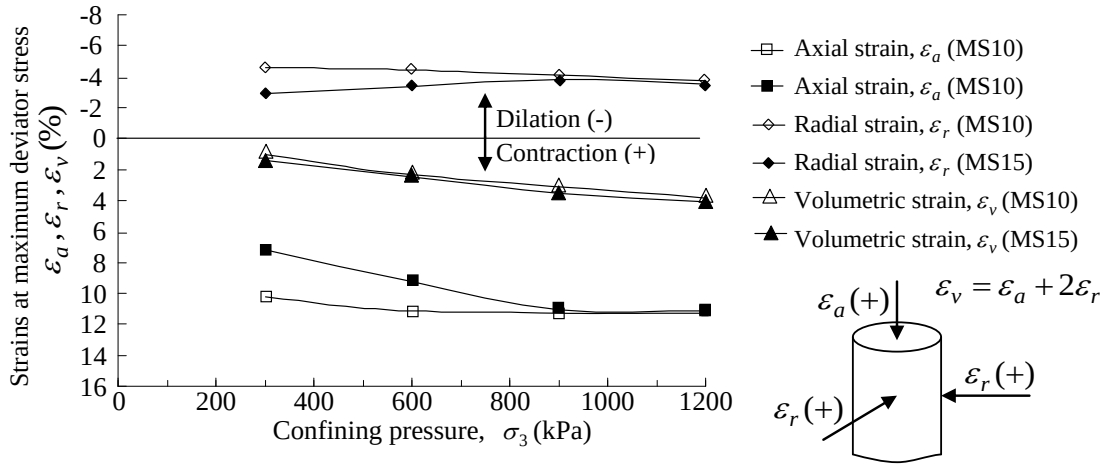

Fig. 6: Variation of specimen strains at peak deviator stress with confining pressures and mudstone contents.

A clear non-linear relationship is present between two parameters (the initial Poisson's ratio υ_i and initial tangent deformation modulus E_i) and confining pressures when specimen A is exposed to low confining pressures compared to high confining pressures (Indraratna et al. 1998). The initial tangent deformation modulus E_i increases along with confining pressures, which indicates the pressure sensitivity nature of rockfill. Compared to the effect of confining pressure on strength, void ratio is more effective in affecting deformation modulus. It was reported (Guo 1999) that deformation modulus E_i varies at around two folds when confining pressures is between 50-1440 kPa, whereas, void ratio change of 0.05 under a constant confining pressure may lead to a deformation modulus E_i variation of 2 folds. Accordingly, an inconsistency between on-site and laboratory compactions may make the experimental data less

reliable. The dry density is required to represent the on-site one. Initial Poisson's ratio υ_i is more profoundly affected by the confining pressure σ_3'. Incensement in confining pressures simply limits the radial strain development, which results in a decreased Poisson's ratio. It is indicated that Poisson's ratio at failure υ_{tf} is readily associated with the dilation ratio at failure $(\Delta\varepsilon_v/\Delta\varepsilon_a)_f$. In general, the Poisson's ratio of rockfill at failure is around 0.5, rarely related to confining pressures (Zhang and Si 1982). In this research, specimens B and C largely follow the identical law.

Shear strength

Fig. 7 presents the Mohr-Coulomb failure envelope line and Mohr circles for specimen MS15. The real strength envelope line is a down-deflexed curve. Shear strength non-linearly increase with normal stress σ_n, but the increment become less. Specifically, factor $\tan\varphi$ decreases with increased σ_n.

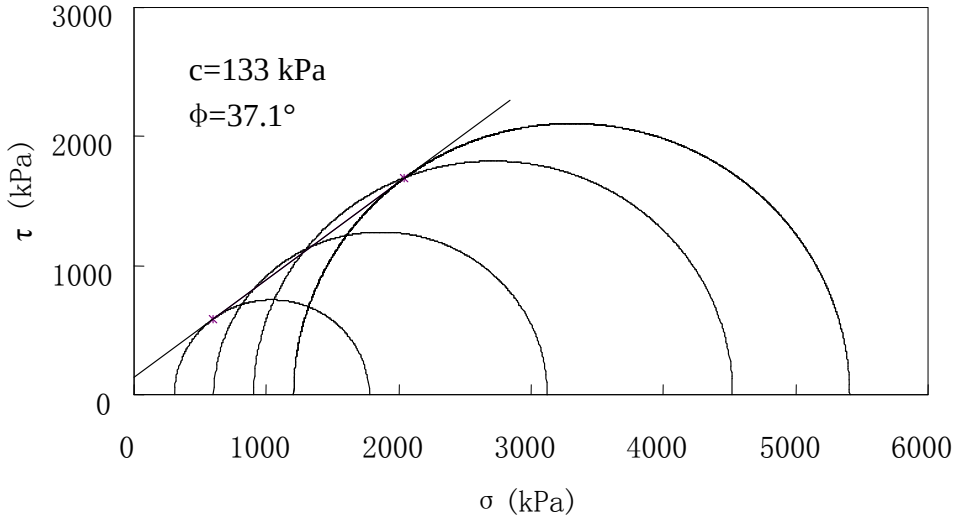

Fig. 7: Mohr-Coulomb failure envelope line and Mohr circles for specimen MS15.

(De Mello 1977)(Zhang and Si 1982) and (Guo 1987) employed exponential functions, e.g. $\tau = A(\sigma_n)^b$, to express the relationship between shear strength τ and normal stress σ_n at failures. (Charles and Watts 1980) thought that these functions applies to limited σ_n, i.e, $(40 < \sigma_n < 400kPa)$. (Charles and Watts 1980) and (Indraratna et al. 1998) related the shear strength nonlinear development to the significant dilation under low normal stresses. In Britain, sandstones were used as rockfill to construct Scammonden Dam and Winscar Dam. The large-size triaxial tests were conducted on rock fill specimens of 23 cm in diameter. It is reported (Guo 1999) the failure envelope line is clearly down-deflexed when the vertical compression is less than 400 kPa. In addition, three characteristics regarding the curves at failure are summarized, i.e., a) larger bending magnitude than sands, b) clear bending under low confining pressure

(<500 kPa), c) a linear relationship between φ_0 and $\lg\sigma_3$. Similar results are obtained in this research.

For specimens A which is tested under low confining pressures $(\sigma_3 > 300kPa)$, the failure envelope line is clearly curved, sourcing from origin. For specimens B and C that are tested under high confining pressures $(\sigma_3 > 300kPa)$, their failure envelope lines are basically linear. It is analyzed that the nonlinear characteristics under low confining pressures is primarily related to the dilation property of granular materials. Under moderate confining pressures, the dilation is offset by the particle broken phenomena. The inter-particle friction prevails, where the middle linear section of the failure envelope line is formed. Under high confining pressures, the dilation effect is further offset. With the pressure exceeding the particle strength tolerance, broken particles fill most of the voids, which offsets the contact pressures between particles. Particles breaks eventually cease. The gradient of the strength envelope lines maintain linearly.

Internal friction angle

Internal friction angle φ' for coarse aggregate is generally expressed as $\sin^{-1}\frac{(\sigma_1'/\sigma_3')_p - 1}{(\sigma_1'/\sigma_3')_p + 1}$. With the increase of confining pressure σ_3', the peak principal stress ratio $(\sigma_1'/\sigma_3')_p$ decreases (Figs. 4 and 5). Accordingly, internal friction

angle φ' decreases with increased σ_3' (Fig. 7), which is also suggested by (Marsal 1967) (Marsal 1973) (Charles and Watts 1980) and (Indraratna et al. 1993). The variation of the internal friction angle may be associated with aggregate gradation, shape and texture. Under low confining pressures, high φ' is caused by the interlocking-based strong shear dilation and minimal aggregate breakage. With the increase of confining pressures, the effect of particle and its gradation is ignorable compared to the effect of confining pressure.

Per the relationship between confining pressure σ_3' and internal friction angle φ' plotted on a semi-logarithmic scale, it is indicated that there is a linear relationship between φ' and $\lg\sigma_3'$. The internal friction angle of rockfill decreases with the confining pressure increase. The relationship is simulated as $\varphi' = \varphi_0 - \Delta\varphi \lg(\sigma_3'/p_a)$, where φ_0 is the internal friction angle under standard atmospheric pressure and is related to the parent rock property, rock nature, grain gradation and shape, density; $\Delta\varphi$ represents the decrement of internal friction angle when confining pressure increases in 10 fold. According to previous triaxial test results, shear strength of rockfill can be presented using the above equation, with parameters φ_0 and $\Delta\varphi$ being equal to 54.4° and 10.4°, respectively (Bo and Cui 1997). In this research, parameters for specimens B and C are $\varphi_0 = 49.6°$, $\Delta\varphi = 8.7°$, and $\varphi_0 = 49.2°$, $\Delta\varphi = 8.9°$, respectively. Although the gradations of specimens B and C are the same, parameter $\Delta\varphi$ of specimen C is

greater than that of specimen B, whereas parameter φ_0 of specimen C is less than that of specimen B. This occurrence is associated with specimens' inconsistency in dry unit weights and mudstone contents. It shall be pointed that road rockfills are poor-graded ($Cu = 12.9$) and dam rockfills are relatively well-graded ($Cu = 45.62$). As a result, the internal friction angle of road rockfills decrease faster with the confining pressure increase than dam rockfills do.

Aggregate breakage characteristics

Under high confining pressures, breakage of coarse aggregate becomes more concerned. Breakage of coarse aggregates affects shear strength and deformation behavior (Qin et al. 2001). Due to the large dimension and being brittle, the gradation, composition and orientation of coarse aggregates vary from time to time depending upon the shearing states. As a result, the stress states among coarse aggregates rearrange and aggregates become more compacted and stable. Research on aggregate breakage was mainly conducted on the breakage level associated with influence factors. Less study was performed on the effects of breakage on shear strengths and stress-strain behaviors, and even constitutive law of coarse aggregates.

Table 1 presents the particle gradations of prepared specimens and tested specimens for MS15. Breakages were observed for aggregates ranging from 5 to 60 mm. No data indicate that aggregates less than 5 mm experience breakage.

Breakages are correlated with confining pressures and particle sizes. More breakages are associated with higher confining pressures and larger particle sizes, which is also reported by (Indraratna et al. 1998).

Table 1: Aggregate breakage characteristics of specimen MS15.

Specimens	Particle sizes (mm) and mass percentages (%)				
	60~40	40~20	20~10	10~5	<5
A	15.00	30.00	22.00	14.00	19.00
B	12.26	22.60	21.82	11.68	31.64
C	8.98	24.05	24.69	12.68	29.60
D	6.54	23.05	22.3	13.25	34.86
E	4.66	23.31	18.91	13.98	39.14

A: prepared specimen, B: tested specimen under σ_3'=300 kPa, C: tested specimen under σ_3'=600 kPa, D: tested specimen under σ_3'=900 kPa, E: tested specimen under σ_3'=1200 kPa.

Under triaxial tests, rockfills behavior clearly different from sands. Rockfills sustain a large number of particle breakages. Many factors contribute to the breakage, e.g., rock minerals, parent rock strength, particle shape, weather degree and stress conditions.

Discussion on coarse aggregate strength and deformation

Rockfills, as a coarse aggregate, are comprised of uneven, heterogeneous granular materials. As rock granular aggregates are not rigid. To bear shear resistance, aggregate must undergo (shear) deformation. On the large, the aggregates vary

volumetrically, either shear dilation or shear contraction. The dilation and contraction is a unique property of granular materials, and is closely related to the physical and mechanics properties. Under triaxial tests, along with the increase of axial stresses, inter-particle relative movement and slippage take place, which converts the granular structure by increasing its bearing capacity. The axial stress increase eventually fails the specimens. The energy generated by confining and axial stresses is partially consumed on the inter-particle friction, dilation, and particle rearrangement. The remaining energy is reserved as elastic energy. Strength and deformation properties of coarse aggregate are thought associated with four factors, i.e., inter-particle friction, dilation, particle rearrange and breakage.

The strength of coarse aggregate are dependent upon the strength of parent rocks. The higher the material's strength, the higher breakage pressure required, and the higher the coarse aggregate's strength. Under low confining pressures, the strong dilation effect of coarse aggregates significantly enhance increase of internal friction angle. The envelope line starts from the origin at a high slope. Under low confining pressures, the dilation effect is offset by the partial particle breakage, and the interlock effect is predominant. (Vesic and Clough 1968) pointed out that when the pressure exceeds the breakage limit, the dilation and void ratio effect are completely inactive. Particle breakage becomes the unique mechanism. (Lee and Seed 1967) thought that the particle breakage mechanism is similar to particle

rearrangement. Particle breakage will absorb much energy. High pressure will causes large failure deformation, which also increases the energy absorption in particle rearrangement. However, once the particle breaks, the original bearing structure is destroyed. The contact pressures are redistributed. As a result, the point-stress is mitigated and averaged, leading to a stable structure. Simultaneously, the internal connection and interlock is offset. Particles are easily movable, which impede the dilation. In addition, as massive particles break, fine contents increase in the structure. When the fine contents attain to a level where coarse particles are separated, coarse aggregates process some behavior of fine soils, leading to strength decrease. This may be the main reason of internal friction angle decrease.

When pressures exceed the particle breakage limit, particle breakages will fill the voids and offset the particle contact pressures. Particles will not undergo breakage any more and tend to be stable. The strength envelope line keeps being linear. Therefore, different factors are affecting strength of coarse aggregate under high and low confining pressures, which explains the decrease of internal friction angle along with confining pressure increase, and the curvature of failure envelope line.

Stress path tests

Fig. 8 presents the stress-strain curves of four stress paths shown in Fig. 3 (a), i.e., four different deviator stress gains after a 900 kPa isotropic consolidation. The "900 k0.125" and "900 k0.333" represent curves for constant principal stress gradient $k = d\sigma_3 / d\sigma_1$ being 0.125 and 0.333, respectively. The "900 C" represents curves for conventional triaxial compression with σ_3 being 900 kPa. The "900 p" represents curves for constant *p* stress path. Varied stress paths lead to different stress-strain curves. To increase minor principal stress σ_3 tends to mitigate the axial strain in the shear processes (Fig. 8 (a)). Axial contractions were observed with strain in the range of 2% to 6%. In Fig. 8 (b), Radial dilations were observed with paths of "900 k0.125", "900 C" and "900 p"; however, radial contraction was observed with path "900 k0.333". It is inferred that minor principal stress gain in the shear processes helps convert radial dilation into radial contraction.

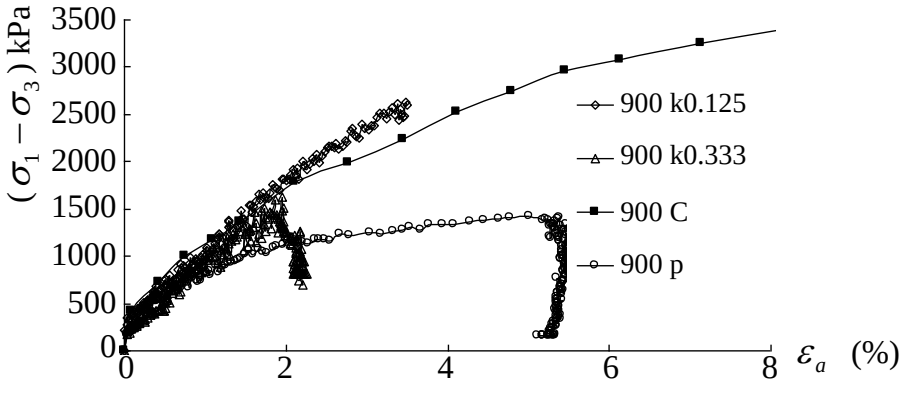
$(\sigma_1-\sigma_3)$ kPa
3500
3000
2500
2000
1500
1000
500
0
0
2
4
6
8
ε_a (%)
900 k0.125
900 k0.333
900 C
900 p

(a)

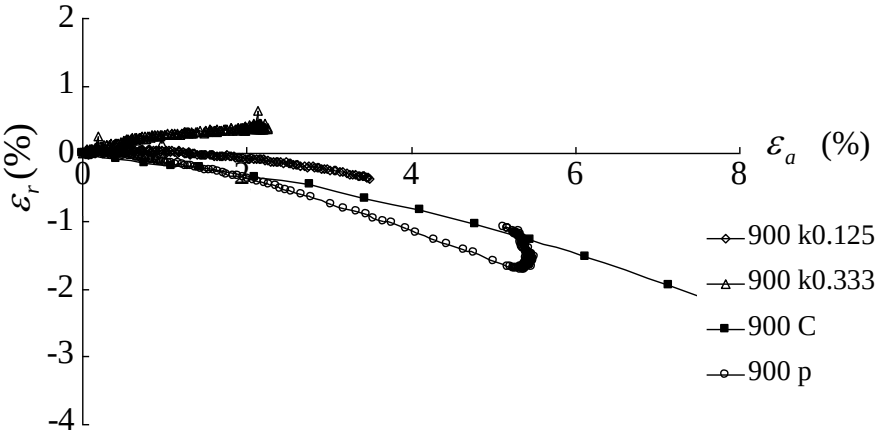
2
1
0
-1
-2
-3
-4
ε_r (%)
0
4
6
8
ε_a (%)
900 k0.125
900 k0.333
900 C
900 p

(b)

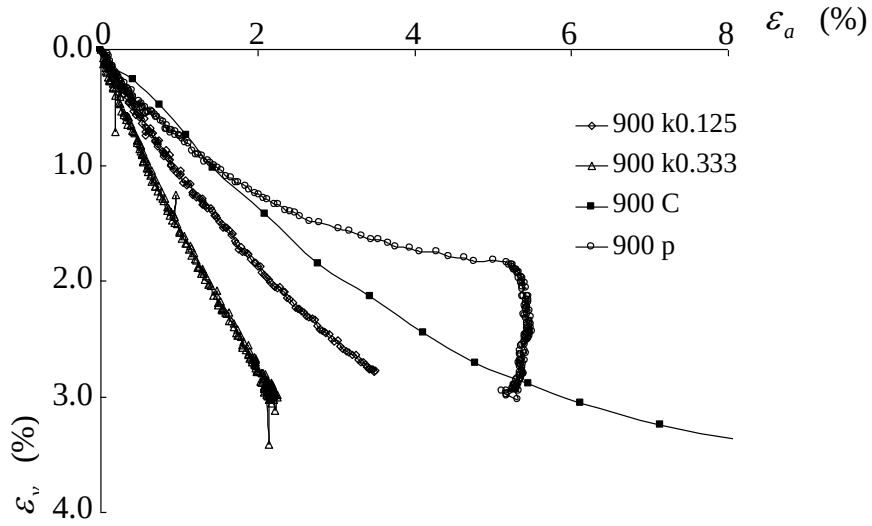

(c)

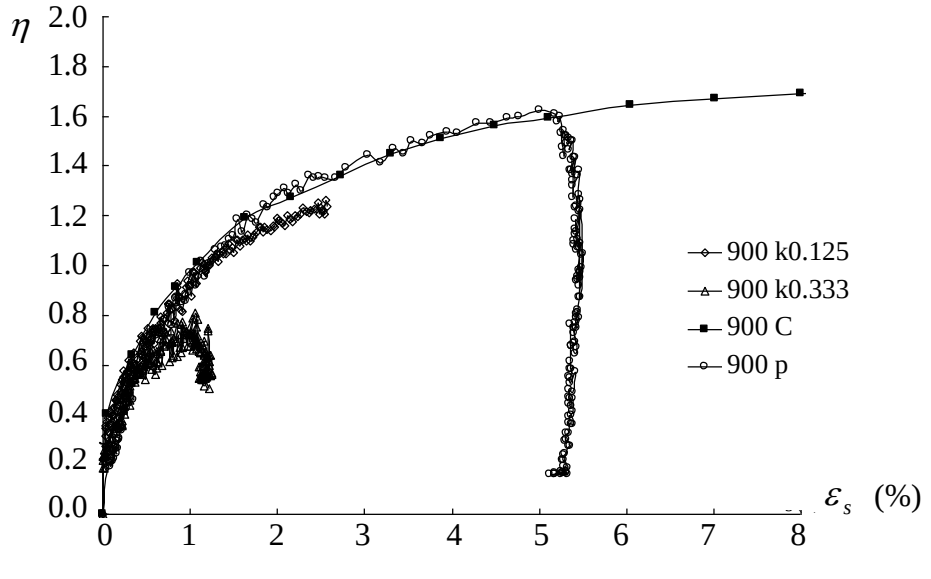

(d)

Fig. 8: Stress-strain curves of constant principal stress gradient *k* (0.125 and 0.333, respectively), conventional triaxial compression and constant *p* stress paths: (a) $(\sigma_1 - \sigma_3) \sim \varepsilon_a$, (b) $\varepsilon_r \sim \varepsilon_a$, (c) $\varepsilon_v \sim \varepsilon_a$, (d) $\eta \sim \varepsilon_s$.

The transition of principal stress gradient *k* exists somewhere between 0.125 and 0.333. In terms of the magnitudes of the radial and axial strain at failure (Fig. 8 (b)), path "900 k0.333" has less strain than path "900 k0.125", indicating a strain

reduction incurred by increasing principal stress gradient k. According to Fig. 8 (c), volumetric contraction of path "900 k0.333" develops relatively fast compared to the other three paths. Minor principal stress thus plays a role in reducing both radial and volumetric dilation strain. Also for path "900 p" in Fig. 8 (a, b and c), with the decrease of minor principal stress and increase of major principal stress, relatively fast axial contraction and radial dilation, but slow volumetric contraction, were identified. It means that constant *p* stress path tends to offset volumetric strain by a transition between axial and radial strains. Four stress paths present similar $\eta \sim \varepsilon_s$ curves (Fig. 8 (d)). In the unloading phase for *k*=0.333 stress path, axial, radial and volumetric contraction increase slightly. No rebound was identified. It is interpreted that aggregates reach stable states after rearrangement and breakage.

Fig. 9 presents stress-strain curves of constant *p* stress paths shown in Fig. 3 (b) and conventional triaxial compressions. Constant *p* stress paths include 600 ("600 p"), 900 ("900 p") and 1500 kPa ("1500 p"). Conventional triaxial compressions include two paths, i.e., minor principle being 600 ("600 C") and 900 kPa ("900 C"), respectively. Varied stress paths lead to different stress-strain curves. In Fig. 9 (a), deviator stresses increase nonlinearly with axial strain. For three constant *p* stress paths, the initial modulus and deviator stress at failure $(\sigma_1 - \sigma_3)_f$ increase with the increase of consolidation-related minor principle stress σ_3. Deviator stresses at failure $(\sigma_1 - \sigma_3)_f$ for "600 p" and "900 p" are

less than those of "600 C" and "900 C", indicating the strength-enhancing effect of σ_3. Radial dilation was identified for all five stress paths (Fig. 9 (b)). For three constant *p* stress, the increase of consolidation pressure tends to mitigate radial dilation. Radial dilations of "600 p" and "900 p" are correspondingly greater than those of "600 C" and "900 C". In Fig. 9 (c), increased consolidation stress causes volumetric strain increase for constant *p* stress paths. The volumetric strains for constant *p* stress paths are less than those of conventional triaxial compressions, which may be offset by relatively greater radial strains for constant *p* stress paths. In the unloading state for "900 p", axial strain did not change much. Radial and volumetric contractions were identified.

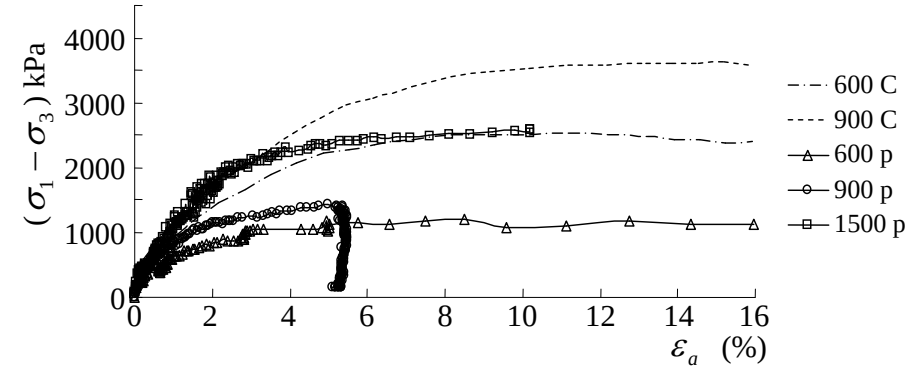
4000
3000
2000
1000
0
$(\sigma_1 - \sigma_3)$ kPa
0
2
4
6
8
10
12
14
16
ε_a (%)
600 C
900 C
600 p
900 p
1500 p

(a)

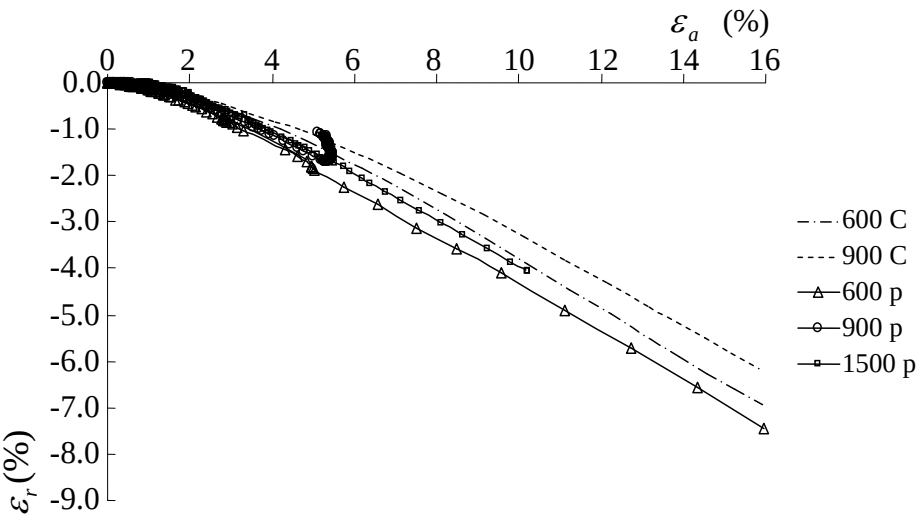
ε_a (%)
0
2
4
6
8
10
12
14
16
0.0
-1.0
-2.0
-3.0
-4.0
-5.0
-6.0
-7.0
-8.0
-9.0
ε_r (%)
600 C
900 C
600 p
900 p
1500 p

(b)

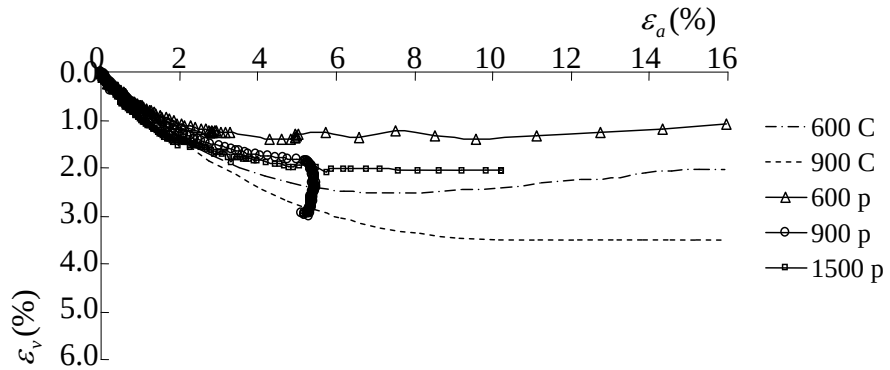

(c)

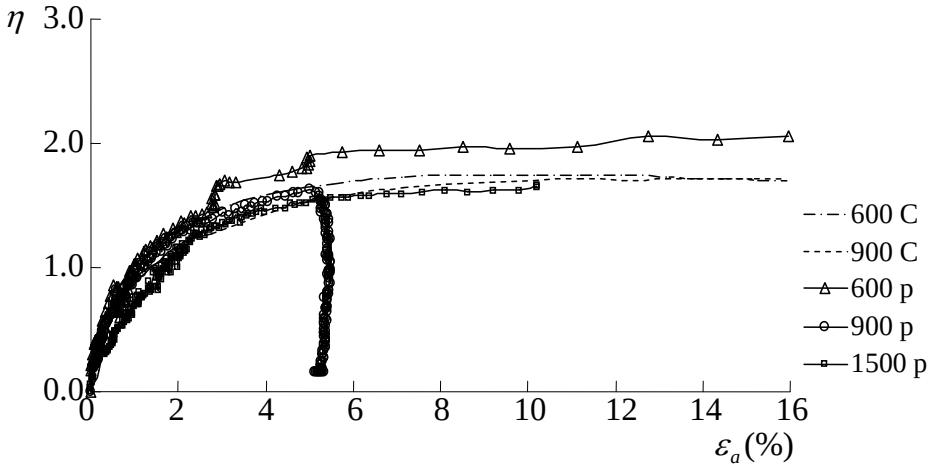

(d)

Fig. 9: Stress-strain curves of constant *p* stress paths and conventional triaxial compressions: (a) $(\sigma_1 - \sigma_3) \sim \varepsilon_a$, (b) $\varepsilon_r \sim \varepsilon_a$, (c) $\varepsilon_v \sim \varepsilon_a$, (d) $\eta \sim \varepsilon_a$.

Fig. 10 presents stress-strain curves of anisotropically consolidated (principal stress ratio k=2.5, 3.0 and 3.5) loading-unloading-reloading stress paths shown in Fig. 3 (c). Deviator stress and volumetric strain increase almost linearly with axial strain in the loading phases (Fig. 10 (a and b)). The greater the principal stress ratio *R*, the less the increasing tendency. That is, with the same axial strain, higher principal stress ratio *R* result in less deviator stress and volumetric strain.

The shear contractions occur along the loading phases (Fig. 10 (b)). In the phase of keeping σ_1 and increasing σ_3, the deviator stress decreases; the volumetric and axial strains increase. With the rise of a reservoir water table, the minor principle stress σ_3 increases and the deviator stress $(\sigma_1 - \sigma_3)$ decreases accordingly. According to Fig. 10 (b), the water rise may cause shear stress decrease and volumetric contraction. (Bo et al. 1999) reported the similar findings that volumetric strain increase 1.03% or 1.83% when σ_1 was keep at 2000 kPa and σ_3 was increased from 800 to 2000. Unloading in constant *p* stress path also causes volumetric contraction.

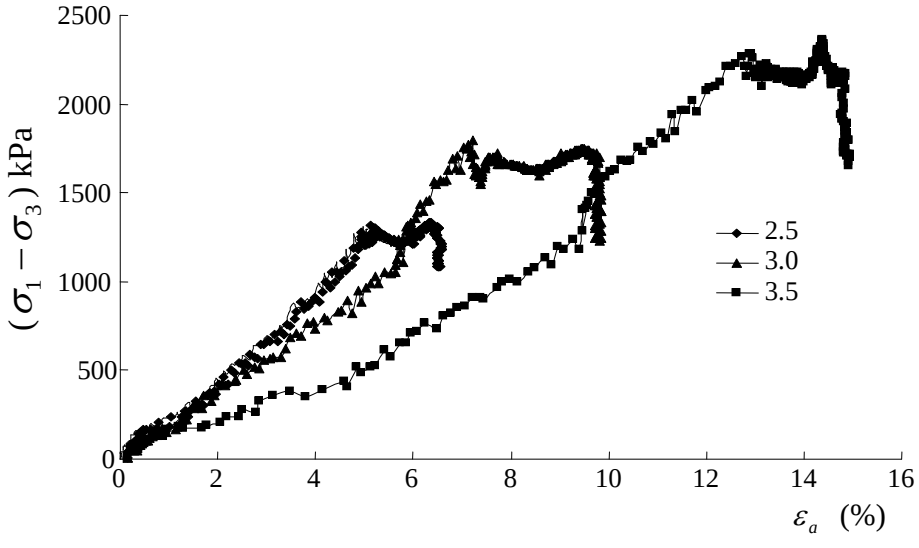

(a)

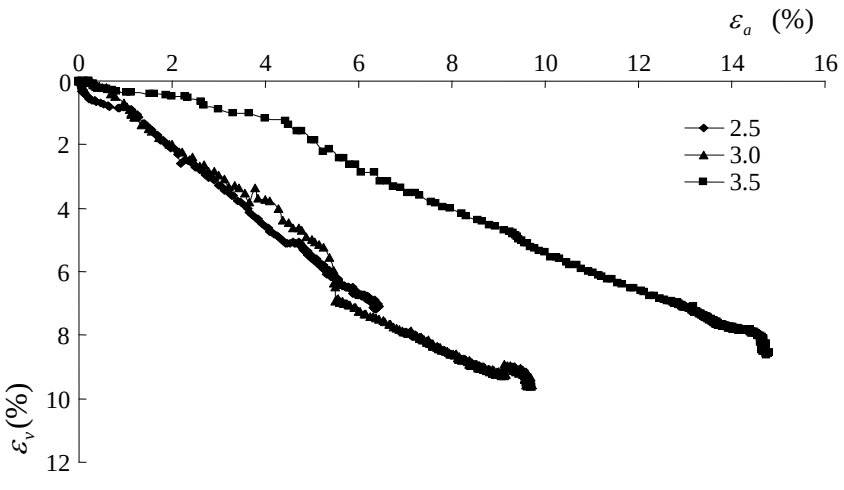
ε_a (%)
0
2
4
6
8
10
12
14
16
ε_v(%)
2.5
3.0
3.5

(b)

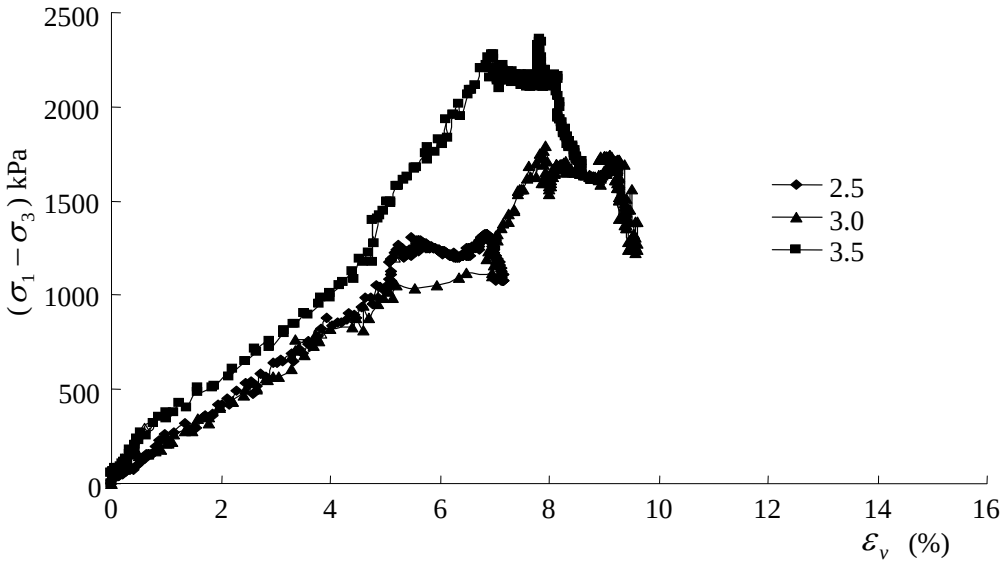
$(\sigma_1-\sigma_3)$ kPa
2500
2000
1500
1000
500
0
ε_v (%)
2.5
3.0
3.5

(c)

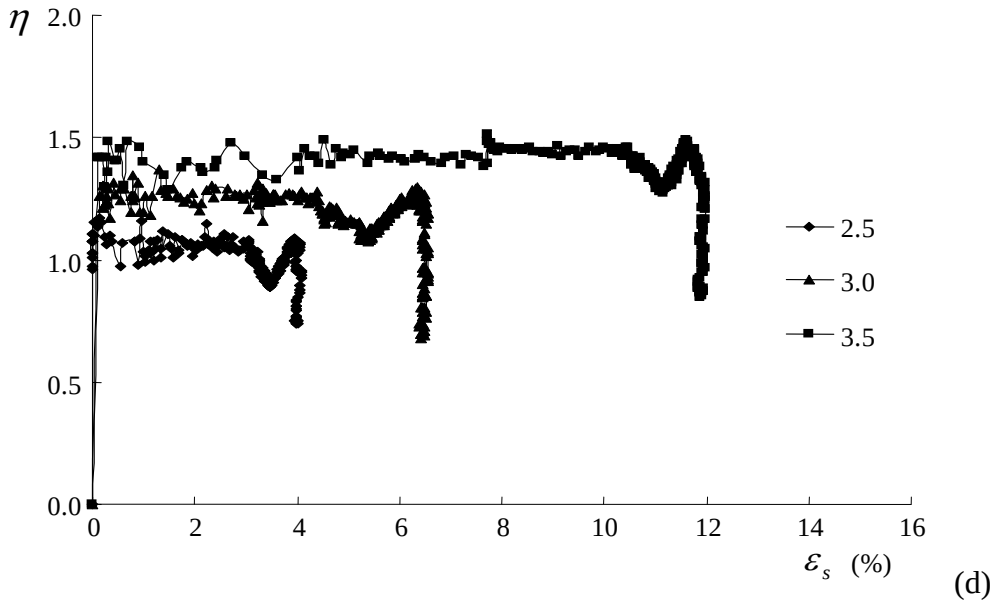

Fig. 10: Stress-strain curves of anisotropically consolidated (principal stress ratio k=2.5, 3.0 and 3.5) loading-unloading-reloading stress paths: (a) $(\sigma_1 - \sigma_3) \sim \varepsilon_a$, (b) $\varepsilon_v \sim \varepsilon_a$, (c) $(\sigma_1 - \sigma_3) \sim \varepsilon_v$, (d) $\eta \sim \varepsilon_s$.

With the decrease of σ_3, shear stress increases. A slight rebound of volumetric strain was observed. In practices, with the fall of reservoir water table, the σ_3 decreases, leading to a stress state of decreased average stress and increased shear stress. In this stage, the aggregates experience a slight dilation. (Bo et al. 1999) reported the similar findings that volumetric strains were -0.08% when σ_1 was keep at 2000 kPa and σ_3 was decreased from 2000 to 800 kPa. The unloading strain is less than that of loading strain. With the increase of σ_3 for the last path, axial strain is almost unchangeable (Fig. 10 (a)). Least volumetric strain occurs (Fig. 10 (c)). The reloading strain is less than that of unloading strain. It

suggests that loading-unloading-reloading process or water rise-fall-rise leads to a decreasing volumetric strain. The elastic deformation becomes less and a plastic deformation is predominating.

The dam construction phase was simulated by constant principle stress ratio *k* loading phases when the major axial deformation occurs. It means that the major of vertical deformation happens in the construction phase.

Fig. 11 presents stress-strain curves of isotropic consolidation (consolidation pressure ε_3 =300, 900 and 1500 kPa) stress paths shown in Fig. 3 (d). Curves of $p \sim \varepsilon_a$, $\varepsilon_v \sim \varepsilon_a$, $p \sim \varepsilon_v$, and $\varepsilon_r \sim \varepsilon_a$ are approximately linear (Fig. 11(a-d)). It means that variables of consolidation pressures, axial, radial and volumetric strains proportionally increase. When the consolidation pressure exceeds 900 kPa, their relationships present a jump, which may indicate that aggregate breakage and rearrangement happen.

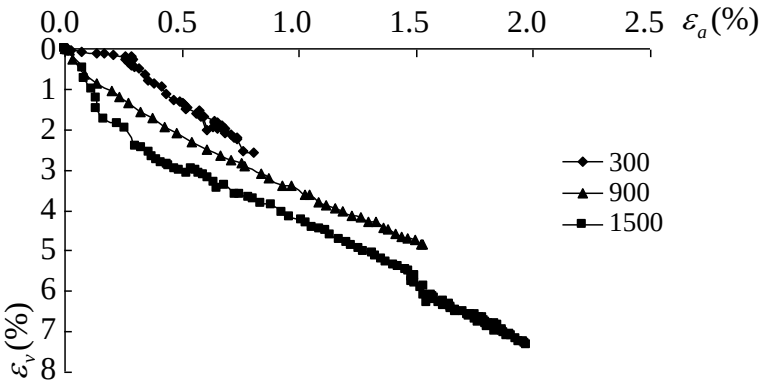
0.0
0.5
1.0
1.5
2.0
2.5
ε_a(%)
0
1
2
3
4
5
6
7
8
ε_v(%)
300
900
1500

(a)

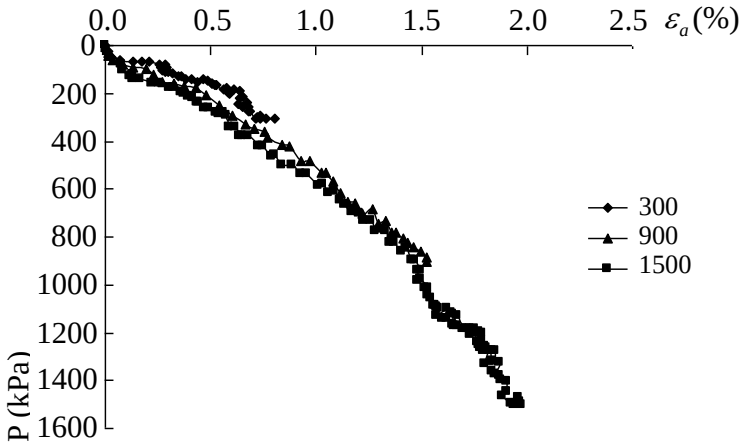
0.0
0.5
1.0
1.5
2.0
2.5
ε_a(%)
0
200
400
600
800
1000
1200
1400
1600
P (kPa)
300
900
1500

(b)

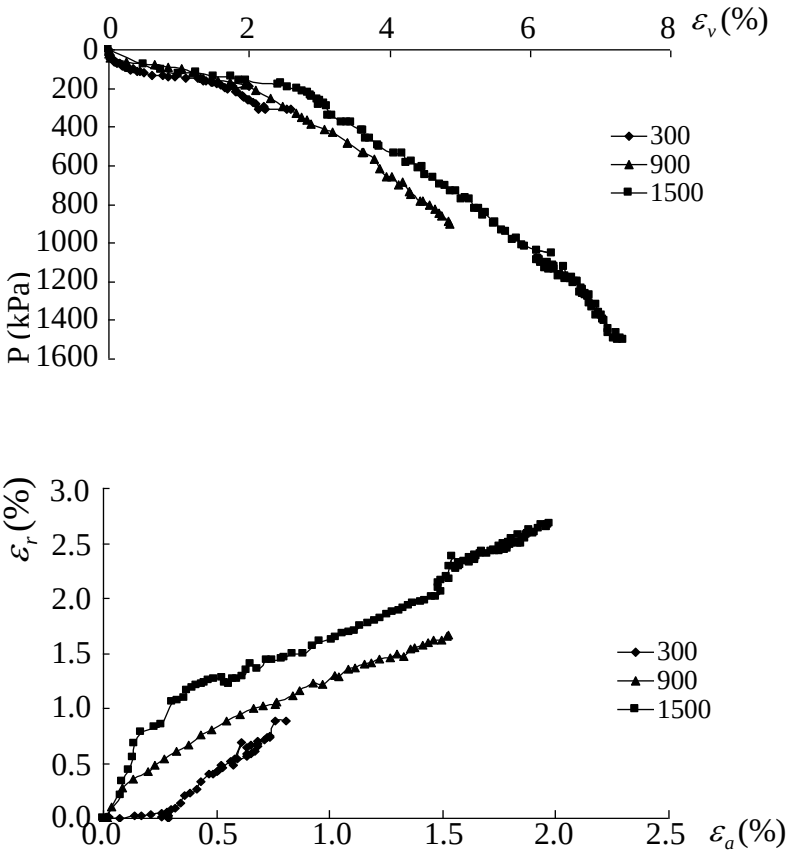

Fig. 11: Isotropic consolidation stress paths: (a) $\varepsilon_v \sim \varepsilon_a$, (b) $p \sim \varepsilon_a$, (c) $p \sim \varepsilon_v$, (d) $\varepsilon_r \sim \varepsilon_a$.

Conclusions

This work is conducted to research the shear behavior of coarse dam aggregates under high confining pressures and varied stress paths, which is critical in the calculation, design, construction and maintenance of high rock fill dams. Coarse rockfills (aggregates) are sampled and tested for their strength and deformation behavior under high and low confining pressures. Mudstones contents are

research about their effect on the mechanical properties of rockfills. Test program includes two aspects, i.e., conventional triaxial tests, stress path triaxial tests. Analyses are focused on the breakage phenomena, mechanism and its effect on strength and deformation of coarse aggregates. Following points are summarized.

Under shear, peak deviator stress increases with confining pressure σ_3' increase. Peak principal stress ratio $(\sigma_1'/\sigma_3')_p$ decrease with confining pressure σ_3' increase. Contraction is firstly introduced, then significant dilation takes place under low confining pressures. With confining pressure increase, the dilation decreases and the contraction eventually prevails. Initial strength parameters (Poisson's ratio υ_i and tangent modulus E_i) presents a nonlinear relationship with confining pressures, if the pressure is relatively low.

Shear strength parameters decrease with increase confining pressures. The failure envelope line is a down-deflexed curve, with clear curvature under low confining pressures. The nonlinear characteristic of failure envelope line is associated with the dilation of coarse aggregate. Under moderate confining pressures, dilation is offset by particle breakage. Under high confining pressures, dilation disappears. Particle breakage continues, with voids filled with fines. The envelope line keeps being linear.

Contents of mudstone are one of important factors affecting rock fill's physical and mechanical properties. Strict controls regarding to the mudstone shall be implemented in actual designs. Deformation behavior of coarse aggregates is also affected by the stress paths. Care shall be placed on conducting well-considered construction procedures in the field. Strength and deformation behavior of coarse aggregates are dependent upon the inter-particle friction, dilation, particle rearrangement and breakage.

Reference

Bishop, W. A. (1966). "The strength of soils as engineering materials". Geotechnique, 16(2): 91-129.

Bo, Shutian and Cui, Yuhao (1997). "Mechanical properties of rockfills." Journal of Hydroelectric Engineering, (3): 21-30. (in Chinese)

Bo, Shutian, Zhou, Xiaoguang and Tao, Huayi (1999). "Effects of stress path on the deformation of rockfill materials." Journal of Hydroelectric Engineering, (4): 76-80. (in Chinese)

Charles, J. A. and Watts, K. S. (1980). "The influence of confining pressure on the strength of compacted rockfill." Geotechnique, 30(4): 353-367.

De. Mello, V. F. B. (1977). "Reflections on design decisions of practical significance to embankment dams." Geotechnique, 27(3): 279-355.

Guo Qingguo (1987). "Shear strength experiments of coarse grained soil." Chinese Journal of Hydraulic, (5): 59-66. (in Chinese)

Guo, Xiling. (1999). In-situ Compaction of Coarse-Grained Materials. Association of Geotechnique of Japan. (in Chinese)

Indraratna, B., Wijewardena, L. S. S. and Balasubramaniam, A. S. (1993) "Large-scale triaxial testing og greywacker rockfill." Geotechnique, 43(1): 37-51.

Indraratna, B., Inoescu, D., and Christie, H. D. (1998). "Shear behavior of railway ballast based on large-scale triaxial tests." Journal of Geotechnical and Geoenvironmental Engineering, 124(5): 439-448.

Lee, K. L. and Seed, H. B. (1967) "Drained strength characteristics of sands." Journal of Geotechnical Engineering, ASCE, 93(6): 117-141.

Marachi, N. D, Chan, C. K. and Seed, H. B. (1972). "Evaluation of properties of rockfill materials." Journal of Soils Mechanics and Foundation Division, ASCE, 98(1): 95-114.

Marsal, R. J. (1967). "Large-scale testing of rockfill materials." Journal of Soils Mechanics and Foundation Division, ASCE, 93(2): 27-43.

Marsal, R. J. (1973). “mechanical properties of rockfill.” Embankment Dam Engineering, Casagrande Volume, New York: Wiley, 109-200.

Ponce, V. M. and Bell, J. M. (1971). “Shear strength of sand at extremely low pressure”. Journal of Soils Mechanics and Foundation Division, ASCE, 97(4): 625-637.

Qin, Hongyu, Shi, Haifeng, Feng, Tugen (2001). “Discussion of several points regarding coarse aggregate large-scale triaxial tests.” Journal of Hohai University, 29 sp: 120-123. (in Chinese)

Vesic, A. S. and Clough, G. W. (1968). “Behavior of granular materials under high stresses”. Journal of Soils Mechanics and Foundation Division, ASCE, 94(3): 661-688.

Wang Qichang. (1999). Civil Engineering in High-speed Railway. Chengdu:Southwest Jiaotong University. (in Chinese)

ZHANG Qi-yue, SI Hong-yang (1982). “Strength and stress strain behaviour of large triaxial compression tests on coarse granular materials.” Chinese Journal of Hydraulic, (9): 22-31. (in Chinese)